Weierstraß-Institut
für Angewandte Analysis und Stochastik

im Forschungsverbund Berlin e.V.

Preprint ISSN 0946 – 8633

Numerical simulation of waves in periodic structures

Matthias Ehrhardt [1], Houde Han and Chunxiong Zheng [2]

submitted: 5th June 2008

[1] Weierstrass Institute for Applied Analysis and Stochastics, Mohrenstrasse 39, 10117 Berlin, Germany
email: ehrhardt@wias-berlin.de

[2] Department of Mathematical Sciences, Tsinghua University, Beijing 100084, P.R. China
email: hhan@math.tsinghua.edu.cn and czheng@math.tsinghua.edu.cn

No. 1323
Berlin 2008

2000 *Mathematics Subject Classification.* 35B27, 65M99, 35Q60, 35J05.

Key words and phrases. periodic media, Helmholtz equation, Schrödinger equation, Dirichlet-to-Neumann maps, Robin-to-Robin maps, band structure, Floquet-Bloch theory, high-order finite elements.

Edited by
Weierstraß-Institut für Angewandte Analysis und Stochastik (WIAS)
Mohrenstraße 39
10117 Berlin
Germany

Fax: + 49 30 2044975
E-Mail: preprint@wias-berlin.de
World Wide Web: http://www.wias-berlin.de/

Abstract. In this work we improve and extend a technique named recursive doubling proceduredeveloped by Yuan and Lu [J. Lightwave Technology 25 (2007), 3649-3656] for solving periodic array problems. It turns out that when the periodic array contains an infinite number of periodic cells, our method gives a fast evaluation of the exact boundary Robin-to-Robin mapping if the wave number is complex, or real but in the stop bands. This technique is also used to solve the time-dependent Schr ödinger equation in both one and two dimensions, when the periodic potential functions have some local defects.

1 Introduction

Nowadays periodic structure problems arise quite often in many modern application areas like semiconductor nanostructures (e.g. quantum dots and nanocrystals), semiconductor superlattices [6], [36], photonic crystal (PC) structures [5], [25], [29], meta materials [31] or Bragg gratings of surface plasmon polariton (SPP) waveguides [18], [32].

The most interesting property of these periodic media, especially in optical applications, is the capability to select the ranges off requencies of the waves that are allowed to pass or blocked in the waveguide ('frequency filter'). Waves in (infinite) periodic media only exist if their frequencies lie inside these allowed continuous bands separated by forbidden gaps. This fact corresponds mathematically to the gap structure of the differential operator having so–called pass bandsand stop bands Numerical simulations are necessary for the design, analysis and finally optimization of the waveguiding periodic structures.

In many cases these wave propagation problems are modeled by periodic partial differential equations (PDEs) on unbounded domains and for solving these equations numerically one has to confine the spatial domain to a bounded computational domain (in a neighborhood of the region of physical interest). *Artificial boundaries* are thus necessary to be introduced and adequate boundary conditions should be imposed. Note that even in the case of a bounded but large domain, it is a common practice to reduce the original domain to a smaller one by introducing artificial boundaries, for example, see [27].

The ideal boundary conditions at the artificial boundaries should not only lead to well–posed problems, but also mimic the perfect absorption of waves leaving the computational domain through the artificial boundaries. Moreover, these boundary conditions should allow for an easy implementation. These boundary conditions are usually called *absorbing* (or transparent, non–reflecting in the same spirit) in the literature. We refer the interested reader to a couple of review papers [3], [14], [16], [17], [35] on this fundamental research topic.

Though *absorbing boundary conditions* (ABCs) for wave-like equations have been a hot research issue for many years and many developments have been made on their designing and implementing, the issue of exact ABCs for periodic structure problems is still not fully-resolved. Some progresses can be found in the recent research articles [9], [10], [12], [13], [23], [30], [33], [34], [38], [39], [40] and [42]. For a review on the theory of waves in locally periodic media including a survey on physical applications we refer the reader to [15].

In the existing literature *frequency domain methods* (FDMs) are usually considered for wave problems with periodic structures [22]. These methods are able to exploit the special geometric structure and are based on an eigenmode expansion in every longitudinally uniform cell. Frequently, the FDMs are used in conjunction with the *perfectly matched layer* (PML) [7] technique for dealing with unbounded domains. Afterwards the *bidirectional beam propagation methods* (BiBPMs) [20] were introduced. Like the FDMs, they can utilize the periodic geometry but additionally they (and also the *eigenmode expansion methods* in [7] and [20]) are able to resolve the multiple reflections at the longitudinal interfaces.

The methods of Jacobsen [21] and Yuan & Lu [38] were developed to be more efficient than the eigenmode expansion methods, because it turns out that solving the eigenmodes in each segment is quite time consuming. More recently, a *DtN mapping method* [37] was developed by Yuan and Lu that is more accurate than the BiBPMs, since this approach works (mostly) without any approximation. In [39] the efficiency of this sequential DtN approach was further improved by a *recursive doubling process* for the DtN map.

In this paper we study a numerical method for the *Helmholtz equation*

$$-\Delta u(\mathbf{x}) + Vu(\mathbf{x}) + zn^2 u(\mathbf{x}) = f(\mathbf{x}). \tag{1.1}$$

Here z is a complex parameter, $V = V(\mathbf{x})$ and $n = n(\mathbf{x})$ are two sufficiently smooth real functions bounded from both below and above. The function n is also positive. The geometry, the functions V and n are assumed to be periodic at least on some part of the

definition domain. In some special cases [21] it is possible to obtain analytic expressions of the solution, but in general, the Helmholtz equation (1.1) has to be solved numerically. If the number of periodic cells is large, then a direct discretization of the whole domain involves a huge number of unknowns which makes it both impractical and costly from an implementational point of view. Our motivation is to find a smart resolution without naively solving the whole domain problem.

The paper is organized as follows. Section 2 is concerned with the Helmholtz equation (1.1) defined on a finite periodic array. An efficient and robust algorithm of the boundary *Robin-to-Robin* (RtR) mapping is presented. This algorithm is then utilized in Section 3 to solve a model waveguide problem. In Section 4 the semi-infinite periodic array problems are considered. It turns out that the algorithm described in Section 2 is very efficient for obtaining the exact boundary RtR mapping if the wave number is complex with nonzero imaginary part or real but in the stop bands. Finally, in Section 5 we discuss the numerical simulation of the time–dependent Schrödinger equation in two space dimensions with a bi–periodic potential function containing a defect.

2 Boundary mappings for arrays periodic in one direction

Let us consider the Helmholtz equation (1.1) under the condition that $V(\mathbf{x}) \equiv 0$ and $f(\mathbf{x}) \equiv 0$, on an array consisting of N identical cells as illustrated in Fig. 1.

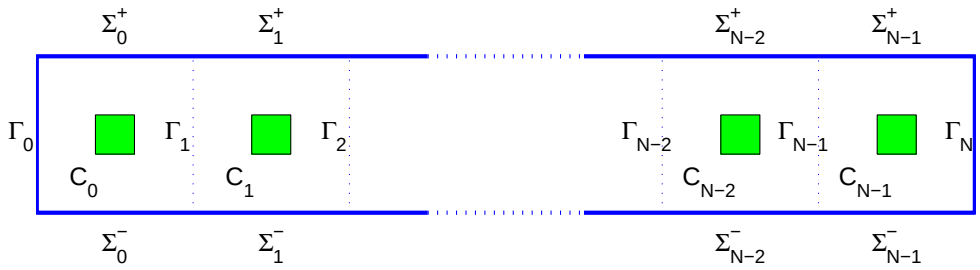

Fig. 1: Schematic view of a periodic array consisting of N cells.

We suppose that *appropriate* homogeneous linear boundary conditions are specified at the upper and lower, and the interior (if existing) boundaries, and these boundary conditions have the same periodicity consistent with that of the periodic structure. Here, "appropriate" means that these boundary conditions do not influence the well–posedness of the interior Helmholtz equation.

We define two *Robin mappings* of u as

$$\mathcal{G}_u^x = (\partial_x + \sqrt[+]{z})u, \qquad \mathcal{F}_u^x = (-\partial_x + \sqrt[+]{z})u.$$

For given boundary data $\mathcal{F}_u^x$ on Γ_i and $\mathcal{G}_u^x$ on Γ_{i+k}, the Helmholtz equation (1.1), together with the boundary conditions on the upper and lower, and the interior (if existing) boundaries, is well–posed on the domain $\cup_{l=i}^{i+k-1} C_l$ (see Lemma A). This implies that

there exist four linear operators $\mathcal{A}_k$, $\mathcal{B}_k$, $\mathcal{C}_k$ and $\mathcal{D}_k$ satisfying

$$\mathcal{G}_u^x|_{\Gamma_i} = \mathcal{A}_k \mathcal{F}_u^x|_{\Gamma_i} + \mathcal{B}_k \mathcal{G}_u^x|_{\Gamma_{i+k}}, \qquad \mathcal{F}_u^x|_{\Gamma_{i+k}} = \mathcal{C}_k \mathcal{F}_u^x|_{\Gamma_i} + \mathcal{D}_k \mathcal{G}_u^x|_{\Gamma_{i+k}}. \tag{2.1}$$

Numerically, these operators can be derived by an appropriate spatial discretization of the domain $\cup_{l=0}^{k-1} C_l$. But if k is big, a large number of unknowns would get involved, which leads to a high computational effort. The task of this section is to design an efficient and robust algorithm for evaluating these operators.

Suppose for $k \in \{m,n\}$, the four linear operators $\mathcal{A}_k$, $\mathcal{B}_k$, $\mathcal{C}_k$ and $\mathcal{D}_k$ have already been obtained. From (2.1) we obtain

$$\begin{aligned}
\mathcal{G}_u^x|_{\Gamma_i} &= \mathcal{A}_m(\mathcal{C}_n \mathcal{F}_u^x|_{\Gamma_{i-n}} + \mathcal{D}_n \mathcal{G}_u^x|_{\Gamma_i}) + \mathcal{B}_m \mathcal{G}_u^x|_{\Gamma_{i+m}}, \\
\mathcal{F}_u^x|_{\Gamma_i} &= \mathcal{C}_n \mathcal{F}_u^x|_{\Gamma_{i-n}} + \mathcal{D}_n(\mathcal{A}_m \mathcal{F}_u^x|_{\Gamma_i} + \mathcal{B}_m \mathcal{G}_u^x|_{\Gamma_{i+m}}).
\end{aligned}$$

According to Lemma B, $I - \mathcal{A}_m \mathcal{D}_n$ and $I - \mathcal{D}_n \mathcal{A}_m$ (I denotes the identity operator) are invertible and thus we have

$$\begin{aligned}
\mathcal{G}_u^x|_{\Gamma_i} &= (I - \mathcal{A}_m \mathcal{D}_n)^{-1} \mathcal{A}_m \mathcal{C}_n \mathcal{F}_u^x|_{\Gamma_{i-n}} + (I - \mathcal{A}_m \mathcal{D}_n)^{-1} \mathcal{B}_m \mathcal{G}_u^x|_{\Gamma_{i+m}}, \\
\mathcal{F}_u^x|_{\Gamma_i} &= (I - \mathcal{D}_n \mathcal{A}_m)^{-1} \mathcal{C}_n \mathcal{F}_u^x|_{\Gamma_{i-n}} + (I - \mathcal{D}_n \mathcal{A}_m)^{-1} \mathcal{D}_n \mathcal{B}_m \mathcal{G}_u^x|_{\Gamma_{i+m}}.
\end{aligned} \tag{2.2}$$

Substituting the above expressions into (2.1) gives

$$\begin{aligned}
\mathcal{G}_u^x|_{\Gamma_{i-n}} &= [\mathcal{A}_n + \mathcal{B}_n(I - \mathcal{A}_m \mathcal{D}_n)^{-1} \mathcal{A}_m \mathcal{C}_n] \mathcal{F}_u^x|_{\Gamma_{i-n}} + \mathcal{B}_n(I - \mathcal{A}_m \mathcal{D}_n)^{-1} \mathcal{B}_m \mathcal{G}_u^x|_{\Gamma_{i+m}}, \\
\mathcal{F}_u^x|_{\Gamma_{i+m}} &= \mathcal{C}_m(I - \mathcal{D}_n \mathcal{A}_m)^{-1} \mathcal{C}_n \mathcal{F}_u^x|_{\Gamma_{i-n}} + [\mathcal{D}_m + \mathcal{C}_m(I - \mathcal{D}_n \mathcal{A}_m)^{-1} \mathcal{D}_n \mathcal{B}_m] \mathcal{G}_u^x|_{\Gamma_{i+m}},
\end{aligned}$$

which imply the relations

$$\begin{aligned}
\mathcal{A}_{m+n} &= \mathcal{A}_n + \mathcal{B}_n(I - \mathcal{A}_m \mathcal{D}_n)^{-1} \mathcal{A}_m \mathcal{C}_n, \qquad \mathcal{B}_{m+n} = \mathcal{B}_n(I - \mathcal{A}_m \mathcal{D}_n)^{-1} \mathcal{B}_m, \\
\mathcal{C}_{m+n} &= \mathcal{C}_m(I - \mathcal{D}_n \mathcal{A}_m)^{-1} \mathcal{C}_n, \qquad \mathcal{D}_{m+n} = \mathcal{D}_m + \mathcal{C}_m(I - \mathcal{D}_n \mathcal{A}_m)^{-1} \mathcal{D}_n \mathcal{B}_m.
\end{aligned} \tag{2.3}$$

Hence, for any fixed cell number N, the operators $\mathcal{A}_N$, $\mathcal{B}_N$, $\mathcal{C}_N$, and $\mathcal{D}_N$ can be obtained by the following steps:

1. Derive $\mathcal{A}_1$, $\mathcal{B}_1$, $\mathcal{C}_1$, and $\mathcal{D}_1$ by the *cell analysis*. If $N = 1$, it is done;

2. Write N into *binary form* $(j_L \cdots j_0)_2$, with $L = [\log_2 N]$ and $j_L = 1$;

3. Use the relations (2.3) L times by setting $m = n = 2^{k-1}$ to get $\mathcal{A}_{2^k}$, $\mathcal{B}_{2^k}$, $\mathcal{C}_{2^k}$, and $\mathcal{D}_{2^k}$ for $k = 1,\ldots,L$;

4. For $l = L-1,\ldots,0$, if $j_l \neq 0$, then use (2.3) by setting $m = (j_L \cdots j_{l+1} 0 \cdots 0)_2$ and $n = 2^l$ to obtain $\mathcal{A}_{(j_L \cdots j_l 0 \cdots 0)_2}$, $\mathcal{B}_{(j_L \cdots j_l 0 \cdots 0)_2}$, $\mathcal{C}_{(j_L \cdots j_l 0 \cdots 0)_2}$ and $\mathcal{D}_{(j_L \cdots j_l 0 \cdots 0)_2}$.

The above procedure uses (2.3) at most $2[\log_2 N]$ times.

Given the boundary data $\mathcal{F}_u^x|_{\Gamma_0}$ and $\mathcal{G}_u^x|_{\Gamma_N}$, in some cases it is necessary to obtain other data in a sub–domain of $\cup_{l=0}^{N-1} C_l$, for example, $\mathcal{F}_u^y|_{\Sigma^-}$ and $\mathcal{G}_u^y|_{\Sigma^-}$ where $\Sigma^- = \cup_{i=0}^{N-1}\Sigma_i^-$. We need only to compute all $\mathcal{F}_u^x|_{\Gamma_i}$ and $\mathcal{G}_u^x|_{\Gamma_{i+1}}$ since for each i they completely determine the function u restricted to C_i. If N happens to be a power of 2, say $N=2^L$, this can be achieved efficiently with the following algorithm:

For $p=L,\ldots,1$ and $k=0,\ldots,2^{L-p}-1$, compute $\mathcal{G}_u^x|_{\Gamma_{k2^p+2^{p-1}}}$ and $\mathcal{F}_u^x|_{\Gamma_{k2^p+2^{p-1}}}$ using (2.2) by setting $i=k2^p+2^{p-1}$ and $n=m=2^{p-1}$.

For a general cell number N, we proceed in the following way:

1. Write N into binary form $(j_L\cdots j_0)_2$, with $L=[\log_2 N]$ and $j_L=1$;

2. For $l=0,\ldots,L$, if $j_l\neq 0$, compute $\mathcal{A}_k$, $\mathcal{B}_k$, $\mathcal{C}_k$, and $\mathcal{D}_k$ for $k=(j_l\cdots j_0)_2$ and $k=N-(j_l\cdots j_0)_2$, and use (2.2) by replacing i,n with $(j_l\cdots j_0)_2$ and m with $N-(j_l\cdots j_0)_2$ to derive $\mathcal{G}_u^x|_{\Gamma_{(j_l\cdots j_0)_2}}$ and $\mathcal{F}_u^x|_{\Gamma_{(j_l\cdots j_0)_2}}$. Then use the algorithm above for a power of 2 to derive $\mathcal{G}_u^x|_{\Gamma_i}$ and $\mathcal{F}_u^x|_{\Gamma_i}$ for any $i=(j_k\cdots j_0)_2+1,\cdots,(j_l\cdots j_0)_2-1$, where k is the largest number satisfying $k<l$ and $j_k\neq 0$.

For any $i=1,\ldots,N-1$, the above algorithm uses (2.3) at most $2[\log_2 N]$ times and (2.2) at most $[\log_2 N]$ times. After all $\mathcal{F}_u^x|_{\Gamma_i}$ and $\mathcal{G}_u^x|_{\Gamma_i}$ are derived, $\mathcal{F}_u^y|_{\Sigma_i^-}$ and $\mathcal{G}_u^y|_{\Sigma_i^-}$ are then obtained by the cell analysis. The final results can be written into the following form

$$\mathcal{G}_u^y|_{\Sigma^-}=(\mathcal{F}\to\mathcal{G})\mathcal{F}_u^x|_{\Gamma_0}+(\mathcal{G}\to\mathcal{G})\mathcal{G}_u^x|_{\Gamma_N},\quad \mathcal{F}_u^y|_{\Sigma^-}=(\mathcal{F}\to\mathcal{F})\mathcal{F}_u^x|_{\Gamma_0}+(\mathcal{G}\to\mathcal{F})\mathcal{G}_u^x|_{\Gamma_N}. \quad (2.4)$$

Here $(\mathcal{F}\to\mathcal{G})$, $(\mathcal{G}\to\mathcal{G})$, $(\mathcal{F}\to\mathcal{F})$ and $(\mathcal{G}\to\mathcal{F})$ are four linear operators defined in suitable distributional spaces.

Remark 2.1. If the boundary condition on Γ_N is given as a *Robin-to-Robin* (RtR) mapping

$$\mathcal{G}_u^x|_{\Gamma_N}=\mathcal{E}_N\mathcal{F}_u^x|_{\Gamma_N}+S_N, \quad (2.5)$$

where $\mathcal{E}_N$ is a linear operator and S_N is a function defined on Γ_N, we have

$$\mathcal{G}_u^x|_{\Gamma_N}=\mathcal{E}_N(I-\mathcal{D}_N\mathcal{E}_N)^{-1}\mathcal{C}_N\mathcal{F}_u^x|_{\Gamma_0}+[I+\mathcal{E}_N(I-\mathcal{D}_N\mathcal{E}_N)^{-1}\mathcal{D}_N]S_N,$$

and

$$\mathcal{G}_u^x|_{\Gamma_0}=[\mathcal{A}_N+\mathcal{B}_N\mathcal{E}_N(I-\mathcal{D}_N\mathcal{E}_N)^{-1}\mathcal{C}_N]\mathcal{F}_u^x|_{\Gamma_0}+[\mathcal{B}_N+\mathcal{B}_N\mathcal{E}_N(I-\mathcal{D}_N\mathcal{E}_N)^{-1}\mathcal{D}_N]S_N. \quad (2.6)$$

The invertibility of $I-\mathcal{D}_N\mathcal{E}_N$ is obvious if the periodic array problem is well–posed with the RtR boundary mapping (2.5) on Γ_N. This expression (2.6) yields an exact RtR mapping at the leftmost boundary Γ_0. Furthermore, if the Dirichlet-to-Neumann (DtN) mapping is well–defined on Γ_0, it can be derived straightforwardly from (2.6).

Remark 2.2. Recently, Yuan and Lu [39] proposed an analogous technique for deriving the exact DtN mapping. In their cell analysis, instead of using Robin data on Γ_i and Γ_{i+1}, they used Dirichlet data to determine Neumann data. A problem will appear if $-z$ happens to be one of the eigenvalues of the operator $-\Delta$ on $\cup_{k=i}^{i+2^J-1} C_k$ for some J with homogeneous Dirichlet boundary conditions specified on Γ_i and Γ_{i+2^J}, since in this case, the Dirichlet-to-Neumann (DtN) mapping does not exist at all. One might argue that the probability for this to happen is very small, but if the total number of periodic cells is large, the eigenvalues of $-\Delta$ with Dirichlet boundary conditions are very dense in the pass bands. This implies that if there are some eigenvalues of $-\Delta$ very close but never equal to s, though the DtN mapping exists, it is very ill-conditioned.

3 Application to Waveguide Problems

In this section we give a first application of the technique proposed in the last section. Consider the Helmholtz equation in the waveguide shown in Fig. 2. The domain between Γ_1 and Γ_2 consists of four periodic cells. Each cell has a size of 1×2 with a hole of 0.5×1 in the center. The domain between Γ_3 and Γ_4 also contains four periodic cells. Each cell has a size of 1×1 with a hole of 0.5×0.5. These two periodic structures are joined with a junction region between Γ_2 and Γ_3. The domains left to Γ_1 and right to Γ_4 are homogeneous.

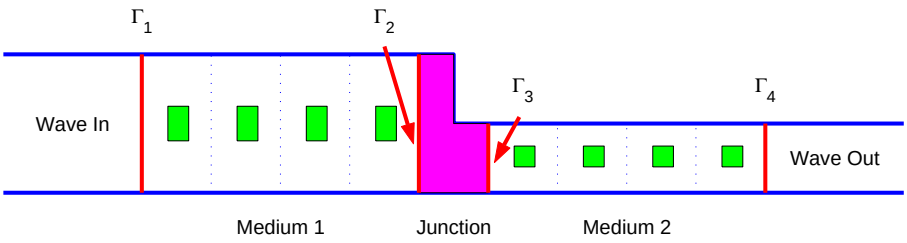

Fig. 2: Schematic view of a model waveguide. Two waveguides with different periodic material properties are joined with a junction zone between Γ_2 and Γ_3.

The governing equation is the Helmholtz equation (1.1) without source term $f(\mathbf{x})$ and $z(\mathbf{x})\equiv -k^2$, i.e.

$$\Delta u + k^2 u = 0, \tag{3.1}$$

where $k>0$ is the real wave number. Zero Dirichlet data is specified on the interior boundaries, and zero Neumann data on the top and bottom boundaries. A plane wave $u_0(x,y)=e^{-ikx}$ is traveling in the waveguide from the left side. It is well–known that the *disturbance part* $u-u_0$ satisfies the left–going boundary condition on Γ_1, i.e.,

$$\frac{\partial}{\partial x}(u-u_0) = \sqrt[+]{-\partial_y^2 - k^2}\,(u-u_0), \quad (x,y)\in\Gamma_1,$$

or equivalently in the form of RtR mapping,

$$\mathcal{F}_u^x = \frac{ik - \sqrt[+]{-\partial_y^2 - k^2}}{ik + \sqrt[+]{-\partial_y^2 - k^2}} \mathcal{G}_u^x + 2iku_0, \quad (x,y) \in \Gamma_1. \tag{3.2}$$

The wave function u satisfies the right–going boundary condition on Γ_4, i.e.,

$$\frac{\partial u}{\partial x} = -\sqrt[+]{-\partial_y^2 - k^2}\, u, \quad (x,y) \in \Gamma_4,$$

or equivalently,

$$\mathcal{G}_u^x = \frac{ik - \sqrt[+]{-\partial_y^2 - k^2}}{ik + \sqrt[+]{-\partial_y^2 - k^2}} \mathcal{F}_u^x, \quad (x,y) \in \Gamma_4. \tag{3.3}$$

Now by using the technique in the last section, we could derive the RtR mapping on Γ_2 and Γ_3. The wave function is then resolved by solving the Helmholtz equation *only* in the junction region between Γ_2 and Γ_3.

To understand the typical wave behaviour in periodic waveguides we must consider the band structure diagrams of the characteristic equation $-\Delta u = \lambda u$ restricted to a single periodic cell. As assumed, the top and bottom boundary conditions are homogeneous Neumann, and the interior boundary condition is homogeneous Dirichlet. The boundary conditions at the left and right boundaries of the single cell are *pseudoperiodic*, namely,

$$u_{\text{right}} = e^{i\theta} u_{\text{left}}, \qquad \partial_x u_{\text{right}} = e^{i\theta} \partial_x u_{\text{left}},$$

where the parameter θ lies in the interval $[0, 2\pi]$. For each value of θ, there exists a sequence of real eigenvalues λ that are shown in the following *band structure diagrams*. These eigenvalues, also regarded as *discrete energies*, correspond to a series of Bloch waves which could travel through the waveguides without damping.

Figs. 3 and 4 show these band structures for the two periodic structures to the left and to the right. The results are obtained by an eighth–order finite element discretization using the step sizes $\Delta x = \Delta y = 0.125$. For the left periodic structure between Γ_1 and Γ_2, the first two stop bands are $(-\infty, 8.27_{\pm 0.01})$ and $(16.69_{\pm 0.01}, 19.49_{\pm 0.01})$, while for the right periodic structure between Γ_3 and Γ_4, they are $(-\infty, 23.61_{\pm 0.01})$ and $(29.85_{\pm 0.01}, 47.10_{\pm 0.01})$. The first eigenvalue of the Dirichlet boundary value problem for the left periodic structure is $19.49_{\pm 0.01}$, while $47.10_{\pm 0.01}$ for the right periodic structure.

We consider in the sequel *five cases*: $k = \sqrt{8}$, $k = \sqrt{19.49}$, $k = 6$, $k = \sqrt{47.10}$ and $k = 8$.

1. $k^2 = 8$ lies in stop bands of both two structures.
2. $k^2 = 19.49$ is the first eigenvalue of the Dirichlet boundary value problem for the left periodic structure.
3. $k^2 = 36$ lies in pass bands of both two structures.

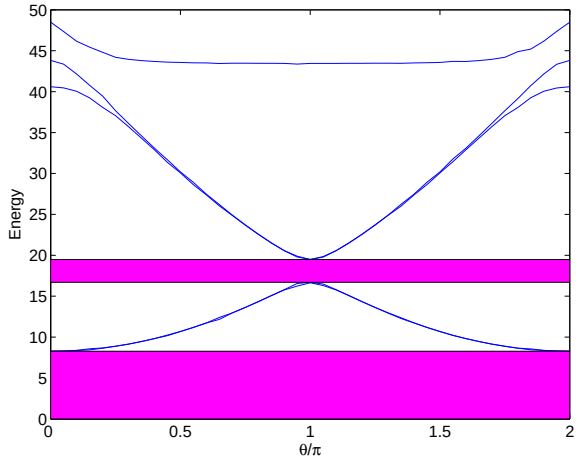

Fig. 3: Band structure with stop bands for the left periodic structure. The first two stop bands are the intervals $(-\infty, 8.27_{\pm 0.01})$ and $(16.69_{\pm 0.01}, 19.49_{\pm 0.01})$

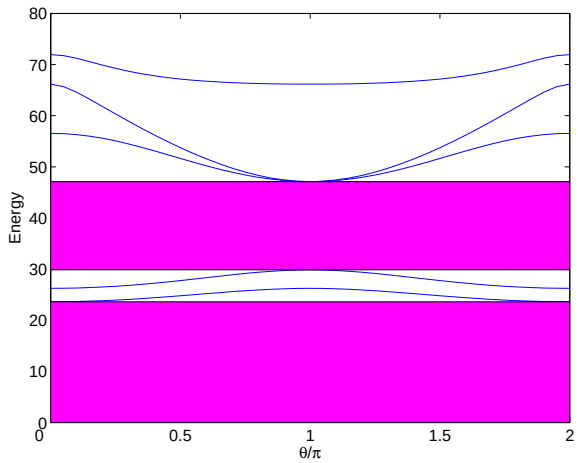

Fig. 4: Band structure with stop bands for the right periodic structure. The first two stop bands are the intervals $(-\infty, 23.61_{\pm 0.01})$ and $(29.85_{\pm 0.01}, 47.10 \pm 0.01)$

4. $k^2=47.10$ is the first eigenvalue of the Dirichlet boundary value problem of the right periodic structure.

5. $k^2=64$ lies in pass bands of both two structures.

We point out the fact that the cases $k=\sqrt{19.49}$ and $k=\sqrt{47.10}$ cannot be solved with Yuan and Lu's method [39] (cf. Remark 2.2). Figs. 5–9 show the real part of the wave function for the five chosen wave numbers. Again an eighth-order finite element code was used in the computation with the step sizes $\Delta x=\Delta y=0.125$.

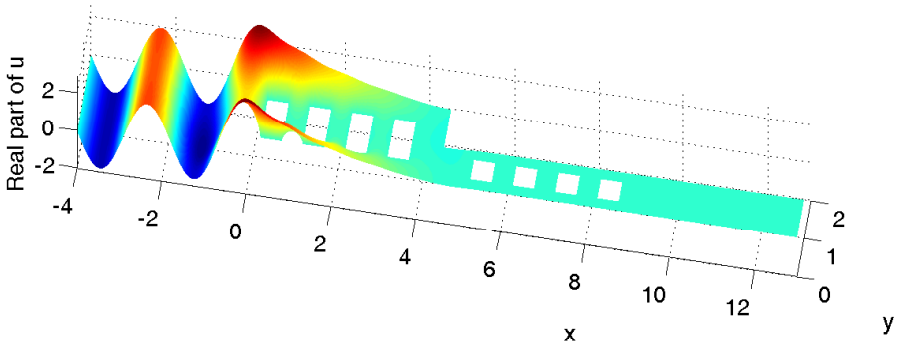

Fig. 5: Real part of the wave function for $k=\sqrt{8}$.

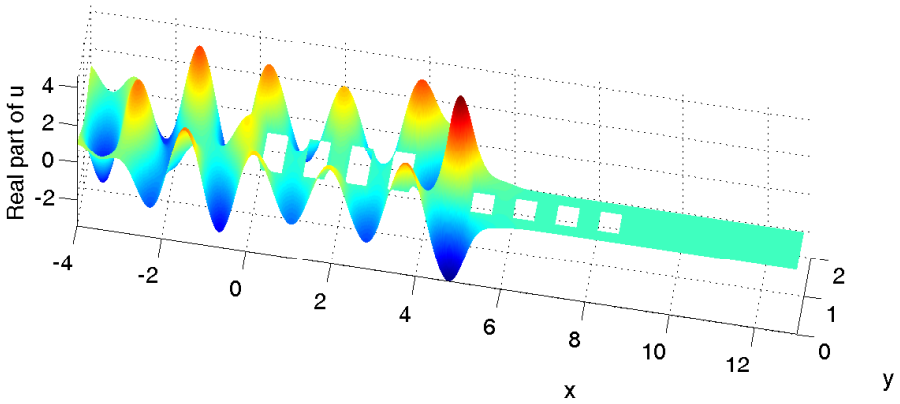

Fig. 6: Real part of the wave function for $k=\sqrt{19.49}$.

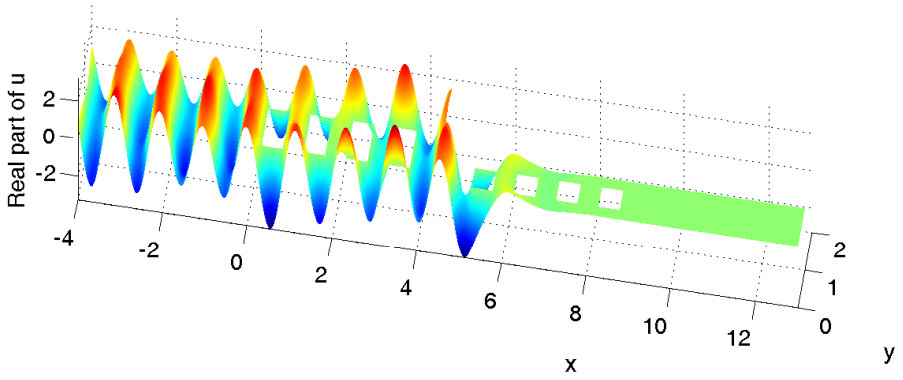

Fig. 7: Real part of the wave function for $k=6$.

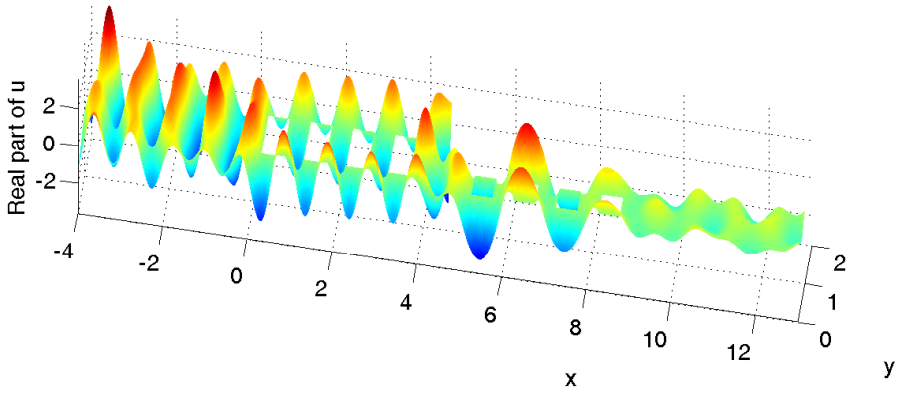

Fig. 8: Real part of the wave function for $k=\sqrt{47.10}$.

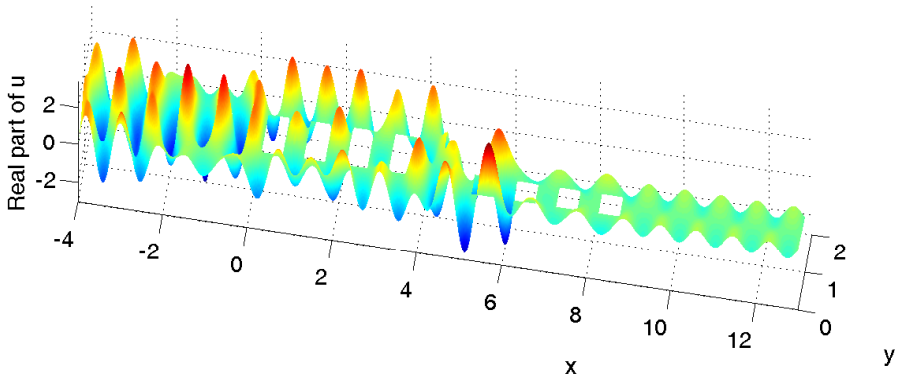

Fig. 9: Real part of the wave function for $k=8$.

4 Exact RtR mapping for semi-infinite periodic array problems

In many cases the exact RtR (thus DtN or DtR) mapping is necessary to handle semi–infinite periodic array problems properly, see Fig. 10. Joly, Li and Fliss [23] presented a Newton-type method for the Helmholtz equation when z has a nonzero imaginary part. In this case any outgoing wave decays to zero exponentially fast at infinity. In Section 2, we have proposed a fast algorithm within $O(\log_2 N)$ operations for obtaining the exact RtR mapping

$$g_0 = \mathcal{A}_N f_0 + \mathcal{B}_N g_N.$$

If the solution decays in one periodic cell with a factor of σ, by setting $N = \lceil -\frac{\ln\epsilon}{\sigma} \rceil$, it is hopeful that $\mathcal{A}_N$ gives an approximation of the exact RtR mapping on Γ_0 with an error of $O(\epsilon)$. Here ϵ denotes the machine precision.

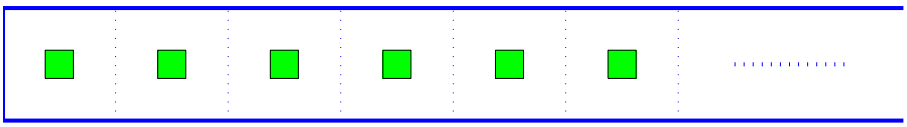

Fig. 10: Schematic view of a semi-infinite periodic array. Each cell has a size of 1×1, and a hole of 0.5×0.5 lies in the center.

It turns out that if $\mathrm{Im}\, z \neq 0$, or z is real but in the stop bands, the operator $\mathcal{A}_N$ converges with an exponential rate to the exact RtR operator. In Fig. 11, we plot the relative errors of $\mathcal{A}_N$ w.r.t. $\mathcal{A}_{ref}$, which is obtained by setting $N = 1024$. In the computation we set $\Delta x = \Delta y = 0.125$ and use an eighth-order finite element method, thus in the discrete level A_N is expressed with a 65-by-65 matrix. Recall that $k^2 = 23{,}31$ are in stop bands, and $k^2 = 25{,}50$ in pass bands, cf. Fig. 4. As a conclusion, using the doubling procedure illustrated in Section 2 at most $J = \lceil \log_2 \lceil -\frac{\ln\epsilon}{\sigma} \rceil \rceil$ times gives the exact RtR boundary mapping at the leftmost boundary up to machine precision. In our numerical tests no instability has been detected even if we set N to as large as 2^{20}. Our technique presents a very fast and robust evaluation of the exact RtR mapping.

If z lies in the stop bands, some traveling Floquet modes would appear, and the above argument ceases to hold. For a well–posed PDE problem, we have to specify the outgoing waves and incoming waves. In a recent work of Joly et al. [23] a method is proposed to resolve this problem. However, we will not discuss this issue in this paper.

As an application, we consider the linear time–dependent Schrödinger equation

$$iu_t + u_{xx} = Vu, \quad x \in \mathbb{R}. \tag{4.1}$$

The initial data $u_0(x)$ and the potential function V are set to be

$$u_0(x) = \exp(-x^2 + ik_0 x), \qquad V(x) = \sum_{n\in\mathbb{Z}, n\neq 0} V_0 \exp(-(x-10n)^2).$$

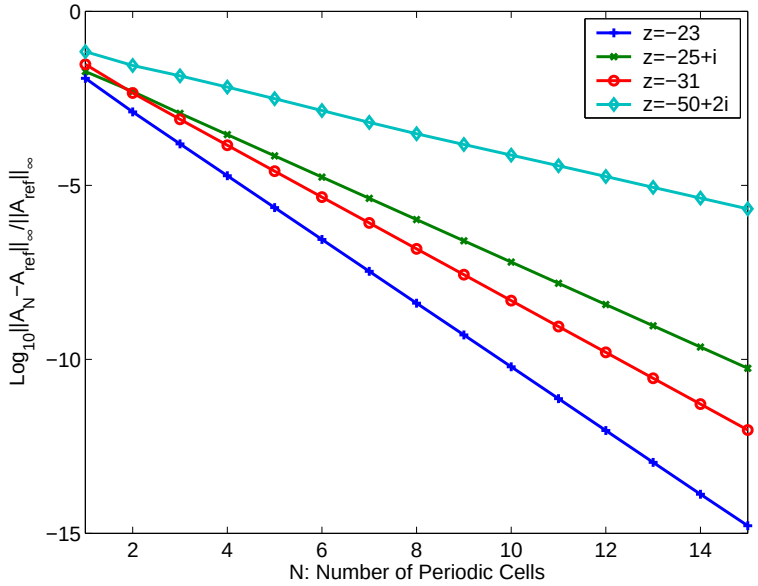

Fig. 11: Convergence of the RtR mapping.

In the Laplace domain the Schrödinger equation (4.1) is transformed into

$$-\hat{u}_{xx}+(V-is)\hat{u}=-iu_0, \quad x\in\mathbb{R}, \tag{4.2}$$

where $\mathrm{Re}\, s>0$ and $\hat{u}$ denotes the Laplace transformation of u defined by

$$\hat{u}(x,s)=\int_0^{+\infty} u(x,t)e^{-st}dt.$$

The function u_0 is well–supported in the interval $[-5,5]$. Outside of $[-5,5]$, the potential function V can be considered periodic with a period of 10. For any fixed s, the equation (4.2) can be solved in $[-5,5]$ with a high–order spatial discretization method. Here we use M eighth–order finite elements, which include $8M+1$ grid points. The RtR boundary conditions at $x=\pm 5$ are derived by the method presented in the beginning of this section. The same number of grid points are used in the discrete periodic cell analysis.

The inverse Laplace transformation is evaluated numerically as

$$u(x,t)=\frac{1}{2\pi i}\int_{\gamma-i\infty}^{\gamma+i\infty} e^{st}\hat{u}(x,s)ds\approx\frac{1}{2\pi}\int_{-f_{\max}}^{f_{\max}}\chi(f)e^{(\gamma+if)t}\hat{u}(x,\gamma+if)df, \tag{4.3}$$

and the integral is further approximated by the middle–point rule. Several parameters need to be tuned: the damping factor γ, the cutoff frequency f_{max}, and the number of quadrature points N_f. In principle, the bigger is γ, the smoother is the function $\hat{u}$, thus the number of quadrature points can be made smaller. But to guarantee stability γ cannot be too large. This is typically because there is an exponential factor $e^{\gamma t}$ involved in the

integral. The *cutoff frequency* f_{max} depends on the regularity of the solution. The smoother is u, the smaller is f_{max}. We leave open the theoretical investigation on the optimal choice of these parameters in this paper. For the considered model problem when $k_0=2$ and $M=16$, we set

$$f_{max}=200, \quad \gamma=1, \quad N_f=1024,$$

and the *filtering function* χ as

$$\chi(f)=\exp\left(-(1.2f/f_{max})^{20}\right).$$

If $V_0=0$, the exact solution is

$$u(x,t)=\sqrt{\frac{i}{-4t+i}}\exp\left(\frac{-ix^2-k_0x+k_0^2t}{-4t+i}\right).$$

The relative L^2–errors in the computational region $[-5,5]$ are listed in Table 1 at different time points. We observe that in this time regime the relative errors are very small. If $V_0\neq 0$, the analytical exact solution is in general not available. In Fig. 12 we illustrate the solution at different time points for $V_0=10$.

Time Point	1.0	1.5	2.0	2.5	3.0	3.5
Relative L^2–Error	1.83(-8)	2.12(-8)	2.66(-8)	3.14(-8)	3.56(-8)	3.92(-8)

Table 1: Relative L^2–errors in $[-5,5]$ at different time points for $V_0=0$.

5 Numerical Simulation of the transient Schrödinger equation in 2D

In this section we consider the following two-dimensional transient Schrödinger equation

$$iu_t+u_{xx}+u_{yy}=Vu,\ \forall(x,y)\in\mathbb{R}^2,\ \forall t>0, \tag{5.1}$$

$$u(x,y,0)=u_0(x,y),\ \forall(x,y)\in\mathbb{R}^2, \tag{5.2}$$

$$u(x,y,t)\to 0,\ r=\sqrt{x^2+y^2}\to+\infty,\ \forall t>0. \tag{5.3}$$

See Fig. 13. The potential function $V=V(x,y)$ is bi-periodic with a periodicity of 1×1 and a defect exists in the center of this periodic structure. The initial data u_0 is assumed locally supported, say in the defect cell.

The definition domain of the above problem is unbounded, and as a first step we could truncate the domain by introducing a rectangular artificial boundary and on it imposing the periodic boundary condition. This treatment is justified if the time interval of

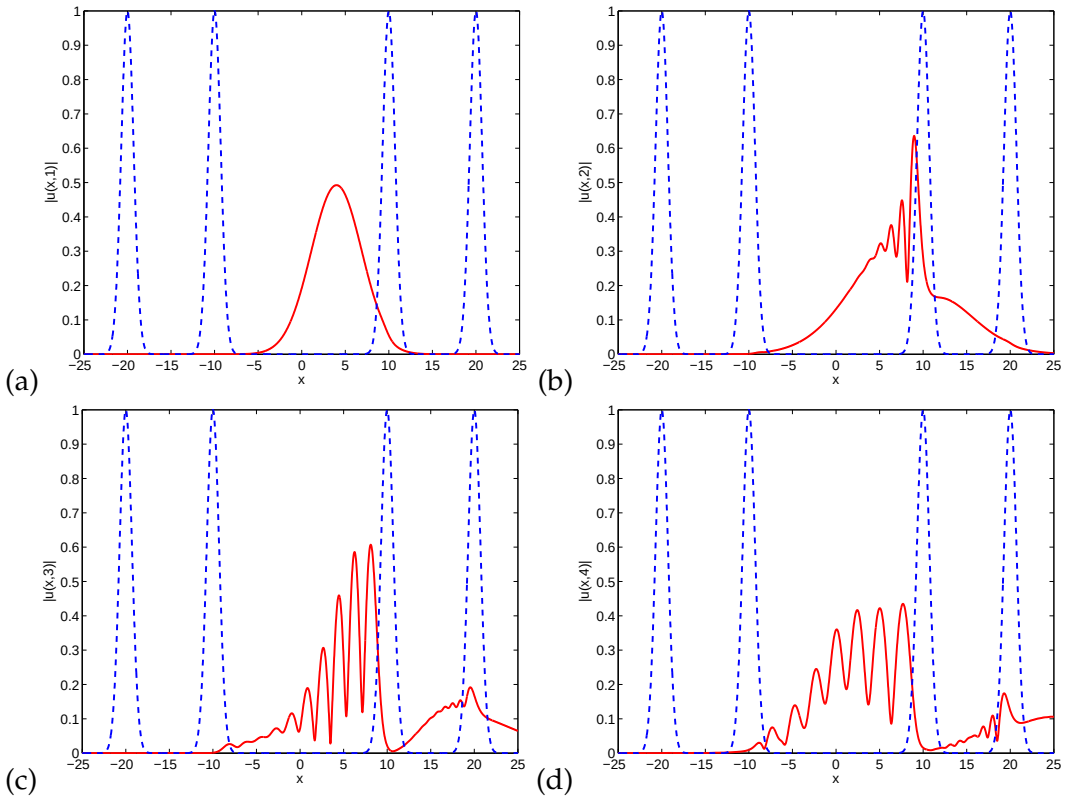

Fig. 12: Evolution of a Gaussian packet in a periodic potential. (a) $t=1$. (b) $t=2$. (c) $t=3$. (d) $t=4$. The dashed blue line shows the potential function scaled by $1/V_0$.

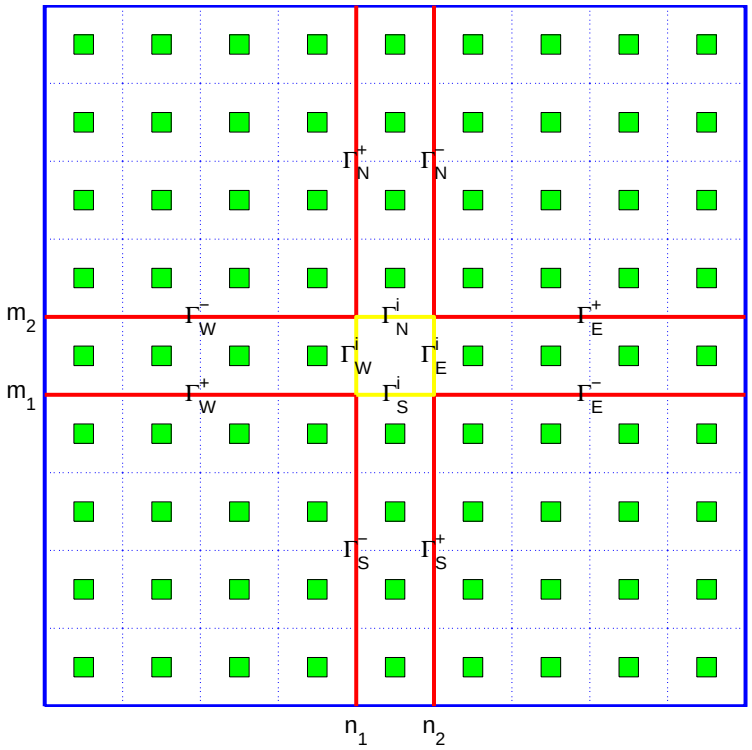

Fig. 13: A bi-periodic potential function with a defect in the center.

simulation is finite and the number of cells enclosed by the artificial boundary is sufficiently large.

The next step is to find a suitable numerical scheme to resolve the wave field. Our basic idea is analogous to that in the last section for handling the one-dimensional Schrödinger equation with periodic potentials at infinity. We first go to the frequency domain by solving the Helmholtz equation

$$-u_{xx}-u_{yy}+(V-is)u=-iu_0 \tag{5.4}$$

with a series of complex parameters s, and then perform the inverse Laplace transformation with a frequency filter. Notice that in (5.4) we use the same notation u to represent its Laplace-transformed function. This is mainly for the brevity of notations used in the following of this section. Of course we do not intend to solve the equation (5.4) on the whole truncated domain, since a large number of unknowns would still get involved. Instead, we try to find an accurate boundary condition on the defect cell boundary $\Gamma_E^i\cup\Gamma_S^i\cup\Gamma_W^i\cup\Gamma_N^i$, and perform computation only on the defect cell.

To arrive at this point, let us first consider the equation (5.4) on the geometry shown in Fig. 14. Suppose periodic boundary conditions are specified on Σ_0 and Σ_M. Set $\Gamma_W=\cup_{k=0}^{M-1}\Gamma_{W,k}$ and $\Gamma_E=\cup_{k=0}^{M-1}\Gamma_{E,k}$. In the y-direction, we have M periodic layers.

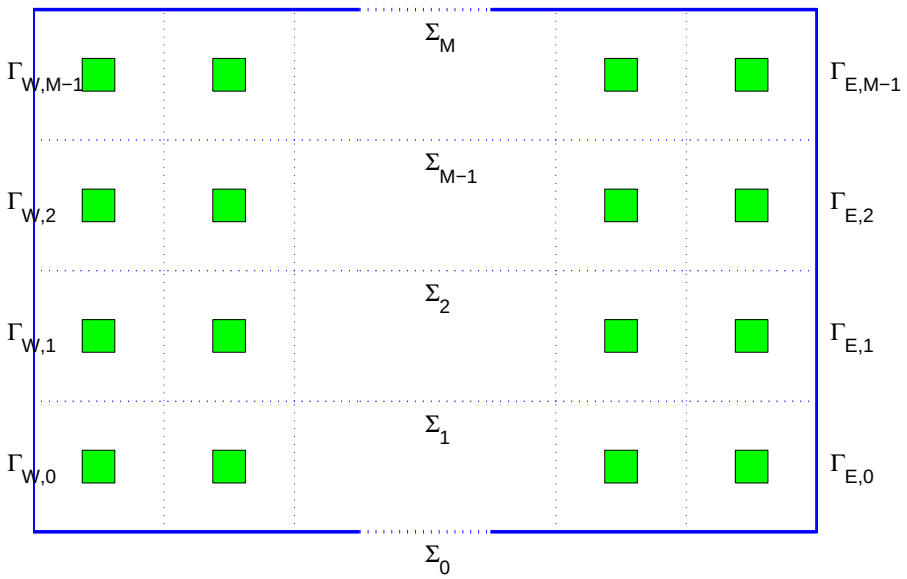

Fig. 14: Schematic view of a bi-periodic structure with periodic boundary conditions specified on Σ_0 and Σ_M.

We define the *discrete Fourier transformation* in the y-direction as

$$\hat{u}_k(x,y)=\sum_{m=0}^{M-1}u(x,y+mL)\omega^{km},\quad \omega=e^{-2i\pi/M},\quad k=0,1,\ldots,M-1.$$

The inverse transformation is given as

$$u(x,y+mL)=\frac{1}{M}\sum_{k=0}^{M-1}\hat{u}_k(x,y)\omega^{-km}.$$

It is straightforward to verify that

$$\hat{u}_k(x,y+L)=\omega^{-k}\hat{u}_k(x,y).$$

Thus the problem on the domain shown in Fig. 14 can be reduced to M periodic array problems with pseudo–periodic boundary conditions on Σ_0 and Σ_1. By the analysis in Section 2, we get

$$\mathcal{G}^x_{\hat{u}_k}|_{\Gamma_{W,0}}=\hat{\mathcal{A}}_k\mathcal{F}^x_{\hat{u}_k}|_{\Gamma_{W,0}}+\hat{\mathcal{B}}_k\mathcal{G}^x_{\hat{u}_k}|_{\Gamma_{E,0}},\qquad \mathcal{F}^x_{\hat{u}_k}|_{\Gamma_{E,0}}=\hat{\mathcal{C}}_k\mathcal{F}^x_{\hat{u}_k}|_{\Gamma_{W,0}}+\hat{\mathcal{D}}_k\mathcal{G}^x_{\hat{u}_k}|_{\Gamma_{E,0}},$$

and

$$\begin{aligned}\mathcal{G}^y_{\hat{u}_k}|_{\Sigma_0}&=(\widehat{\mathcal{F}\to\mathcal{G}})_k\mathcal{F}^x_{\hat{u}_k}|_{\Gamma_{W,0}}+(\widehat{\mathcal{G}\to\mathcal{G}})_k\mathcal{G}^x_{\hat{u}_k}|_{\Gamma_{E,0}},\\ \mathcal{F}^y_{\hat{u}_k}|_{\Sigma_0}&=(\widehat{\mathcal{F}\to\mathcal{F}})_k\mathcal{F}^x_{\hat{u}_k}|_{\Gamma_{W,0}}+(\widehat{\mathcal{G}\to\mathcal{F}})_k\mathcal{G}^x_{\hat{u}_k}|_{\Gamma_{E,0}}.\end{aligned}$$

Then going back to the variable u of (5.4) yields

$$\mathcal{G}^x_u|_{\Gamma_{W,m}}=\mathcal{A}^m\mathcal{F}^x_u|_{\Gamma_W}+\mathcal{B}^m\mathcal{G}^x_u|_{\Gamma_E},\qquad \mathcal{F}^x_u|_{\Gamma_{E,m}}=\mathcal{C}^m\mathcal{F}^x_u|_{\Gamma_W}+\mathcal{D}^m\mathcal{G}^x_u|_{\Gamma_E},$$

and

$$\begin{aligned}\mathcal{G}^y_u|_{\Sigma_m}&=(\mathcal{F}\to\mathcal{G})_m\mathcal{F}^x_u|_{\Gamma_W}+(\mathcal{G}\to\mathcal{G})_m\mathcal{G}^x_u|_{\Gamma_E},\\ \mathcal{F}^y_u|_{\Sigma_m}&=(\mathcal{F}\to\mathcal{F})_m\mathcal{F}^x_u|_{\Gamma_W}+(\mathcal{G}\to\mathcal{F})_m\mathcal{G}^x_u|_{\Gamma_E},\end{aligned}$$

where

$$\begin{aligned}\mathcal{A}^m\mathcal{F}^x_u|_{\Gamma_W}&=\frac{1}{M}\sum_{n=0}^{M-1}\left[\sum_{k=0}^{M-1}\hat{\mathcal{A}}_k\omega^{k(n-m)}\right]\mathcal{F}^x_u|_{\Gamma_{W,n}},\\ \mathcal{B}^m\mathcal{G}^x_u|_{\Gamma_E}&=\frac{1}{M}\sum_{n=0}^{M-1}\left[\sum_{k=0}^{M-1}\hat{\mathcal{B}}_k\omega^{k(n-m)}\right]\mathcal{G}^x_u|_{\Gamma_{E,n}},\\ \mathcal{C}^m\mathcal{F}^x_u|_{\Gamma_W}&=\frac{1}{M}\sum_{n=0}^{M-1}\left[\sum_{k=0}^{M-1}\hat{\mathcal{C}}_k\omega^{k(n-m)}\right]\mathcal{F}^x_u|_{\Gamma_{W,n}},\\ \mathcal{D}^m\mathcal{G}^x_u|_{\Gamma_E}&=\frac{1}{M}\sum_{n=0}^{M-1}\left[\sum_{k=0}^{M-1}\hat{\mathcal{D}}_k\omega^{k(n-m)}\right]\mathcal{G}^x_u|_{\Gamma_{E,n}},\end{aligned}$$

and

$$
\begin{aligned}
(\mathcal{F}\to\mathcal{G})_m\mathcal{F}_u^x|_{\Gamma_W} &= \frac{1}{M}\sum_{n=0}^{M-1}\left[\sum_{k=0}^{M-1}(\widehat{\mathcal{F}\to\mathcal{G}})_k\omega^{k(n-m)}\right]\mathcal{F}_u^x|_{\Gamma_{W,n}},\\
(\mathcal{G}\to\mathcal{G})_m\mathcal{G}_u^x|_{\Gamma_E} &= \frac{1}{M}\sum_{n=0}^{M-1}\left[\sum_{k=0}^{M-1}(\widehat{\mathcal{G}\to\mathcal{G}})_k\omega^{k(n-m)}\right]\mathcal{G}_u^x|_{\Gamma_{E,n}},\\
(\mathcal{F}\to\mathcal{F})_m\mathcal{F}_u^x|_{\Gamma_W} &= \frac{1}{M}\sum_{n=0}^{M-1}\left[\sum_{k=0}^{M-1}(\widehat{\mathcal{F}\to\mathcal{F}})_k\omega^{k(n-m)}\right]\mathcal{F}_u^x|_{\Gamma_{W,n}},\\
(\mathcal{G}\to\mathcal{F})_m\mathcal{G}_u^x|_{\Gamma_E} &= \frac{1}{M}\sum_{n=0}^{M-1}\left[\sum_{k=0}^{M-1}(\widehat{\mathcal{G}\to\mathcal{F}})_k\omega^{k(n-m)}\right]\mathcal{G}_u^x|_{\Gamma_{E,n}}.
\end{aligned}
$$

Note that the above operators can be evaluated efficiently by FFT.

Now come back to the equation (5.4) on the geometry shown in Fig. 13. Since periodic boundary conditions are specified on the boundary of the truncated domain, applying the above analysis we have

$$
\begin{aligned}
\mathcal{G}_u^y|_{\Gamma_E^-\cup\Gamma_W^+} &= (\mathcal{F}\to\mathcal{G})_{m_1}^H\mathcal{F}_u^x|_{\Gamma_S^+\cup\Gamma_E^i\cup\Gamma_N^-} + (\mathcal{G}\to\mathcal{G})_{m_1}^H\mathcal{G}_u^x|_{\Gamma_S^-\cup\Gamma_W^i\cup\Gamma_N^+},\\
\mathcal{F}_u^y|_{\Gamma_E^+\cup\Gamma_W^-} &= (\mathcal{F}\to\mathcal{F})_{m_2}^H\mathcal{F}_u^x|_{\Gamma_S^+\cup\Gamma_E^i\cup\Gamma_N^-} + (\mathcal{G}\to\mathcal{F})_{m_2}^H\mathcal{G}_u^x|_{\Gamma_S^-\cup\Gamma_W^i\cup\Gamma_N^+},\\
\mathcal{G}_u^x|_{\Gamma_N^+\cup\Gamma_S^-} &= (\mathcal{F}\to\mathcal{G})_{n_1}^V\mathcal{F}_u^y|_{\Gamma_W^-\cup\Gamma_N^i\cup\Gamma_E^+} + (\mathcal{G}\to\mathcal{G})_{n_1}^V\mathcal{G}_u^y|_{\Gamma_W^+\cup\Gamma_S^i\cup\Gamma_E^-},\\
\mathcal{F}_u^x|_{\Gamma_N^-\cup\Gamma_S^+} &= (\mathcal{F}\to\mathcal{F})_{n_2}^V\mathcal{F}_u^y|_{\Gamma_W^-\cup\Gamma_N^i\cup\Gamma_E^+} + (\mathcal{G}\to\mathcal{F})_{n_2}^V\mathcal{G}_u^y|_{\Gamma_W^+\cup\Gamma_S^i\cup\Gamma_E^-},
\end{aligned}
\tag{5.5}
$$

and

$$
\begin{aligned}
\mathcal{G}_u^x|_{\Gamma_E^i} &= \mathcal{A}_{m_1}^H\mathcal{F}_u^x|_{\Gamma_S^+\cup\Gamma_E^i\cup\Gamma_N^-} + \mathcal{B}_{m_1}^H\mathcal{G}_u^x|_{\Gamma_S^-\cup\Gamma_W^i\cup\Gamma_N^+},\\
\mathcal{F}_u^x|_{\Gamma_W^i} &= \mathcal{C}_{m_1}^H\mathcal{F}_u^x|_{\Gamma_S^+\cup\Gamma_E^i\cup\Gamma_N^-} + \mathcal{D}_{m_1}^H\mathcal{G}_u^x|_{\Gamma_S^-\cup\Gamma_W^i\cup\Gamma_N^+},\\
\mathcal{G}_u^y|_{\Gamma_N^i} &= \mathcal{A}_{n_1}^V\mathcal{F}_u^y|_{\Gamma_W^-\cup\Gamma_N^i\cup\Gamma_E^+} + \mathcal{B}_{n_1}^V\mathcal{G}_u^y|_{\Gamma_W^+\cup\Gamma_S^i\cup\Gamma_E^-},\\
\mathcal{F}_u^y|_{\Gamma_S^i} &= \mathcal{C}_{n_1}^V\mathcal{F}_u^y|_{\Gamma_W^-\cup\Gamma_N^i\cup\Gamma_E^+} + \mathcal{D}_{n_1}^V\mathcal{G}_u^y|_{\Gamma_W^+\cup\Gamma_S^i\cup\Gamma_E^-}.
\end{aligned}
\tag{5.6}
$$

Here we use the superscripts H and V to distinguish those operators in two different directions. Given $\mathcal{F}_u^x|_{\Gamma_E^i}$, $\mathcal{G}_u^x|_{\Gamma_W^i}$, $\mathcal{F}_u^y|_{\Gamma_N^i}$ and $\mathcal{G}_u^x|_{\Gamma_S^i}$, in principle $\mathcal{G}_u^y|_{\Gamma_E^-\cup\Gamma_W^+}$, $\mathcal{F}_u^y|_{\Gamma_E^+\cup\Gamma_W^-}$, $\mathcal{G}_u^x|_{\Gamma_N^+\cup\Gamma_S^-}$ and $\mathcal{F}_u^x|_{\Gamma_N^-\cup\Gamma_S^+}$ can be determined by the operator equations (5.5). Thus then (5.6) implicitly define a RtR mapping from $\mathcal{F}_u^x|_{\Gamma_E^i}$, $\mathcal{G}_u^x|_{\Gamma_W^i}$, $\mathcal{F}_u^y|_{\Gamma_N^i}$ and $\mathcal{G}_u^x|_{\Gamma_S^i}$, to $\mathcal{G}_u^x|_{\Gamma_E^i}$, $\mathcal{F}_u^x|_{\Gamma_W^i}$, $\mathcal{G}_u^y|_{\Gamma_N^i}$ and $\mathcal{F}_u^x|_{\Gamma_S^i}$. A DtN mapping can be further derived on the boundary of the defect cell, and the computation can now be performed solely on the defect cell.

Unlike the periodic array problems which are periodic only in one direction, the derivation of RtR mapping becomes much more complicated. On the discrete level we need to solve a linear system with unknowns $\mathcal{G}_u^y|_{\Gamma_E^-\cup\Gamma_W^+}$, $\mathcal{F}_u^y|_{\Gamma_E^+\cup\Gamma_W^-}$, $\mathcal{G}_u^x|_{\Gamma_N^+\cup\Gamma_S^-}$ and $\mathcal{F}_u^x|_{\Gamma_N^-\cup\Gamma_S^+}$.

This operation is still much time–consuming. However, if the size of domain is enlarged, the number of unknowns is only increased *linearly* for two–dimensional problems.

We now present a numerical test. The initial function is

$$u_0(x,y) = \exp(-100x^2 - 100y^2 + 20xi).$$

The potential function is

$$V(x,y) = \sum_{m,n\in\mathbb{Z}} V_0 \exp(-100(x-m)^2 - 100(y-n)^2) - V_0 \exp(-100x^2 - 100y^2).$$

The periodic cell is of size 1×1, and the origin is located in the center of the defect cell $[-0.5,0.5]\times[-0.5,0.5]$. The whole computational domain contains $9\times 9=81$ periodic cells. We set the cut-off frequency as 40000, and use the middle–point quadrature rule to approximate the integral (4.3). The number of quadrature points is 1024. Each cell is discretized into $8\times 8=64$ eighth–order finite elements. In Table 2 we list the relative L^2–errors at different time points when $V_0 = 0$. The reference solution is obtained by the spectral method with same grid points. We see that in this time regime, the errors are always less than 0.02 percent. In Figs. 15–18, we show several snapshots for the modulus of wave functions when $V_0 = 0$, and in Figs. 19–22 for the potential $V_0 = 4000$. Note that only 9 cells including the defect cell are shown in those figures.

Time Point ($\times 0.0125$)	1.0	1.5	2.0	2.5	3.0
Relative L^2–Error	4.05(-5)	6.21(-5)	8.65(-5)	1.19(-4)	1.51(-4)

Table 2: Relative L^2–errors in $[-0.5,0.5]^2$ at different time points for $V_0 = 0$.

Conclusion

In this work we introduced a fast evaluation method of the Robin-to-Robin (RtR) mappings for periodic structure problems. Our method is an improvement of the recently developed recursive doubling procedure by Yuan and Lu for the evaluation of Dirichlet-to-Neumann (DtN) maps. The advantage of using RtR rather than DtN mapping lies in the fact that with the former the possibility of encountering some characteristic wave numbers are effectively avoided. This point is very important when considering periodic arrays with a large or infinite number of periodic cells.

It turns out that when the wave number is complex, or real but in the stop bands of the periodic structures, our method can be used to derive the boundary RtR mapping with arbitrary accuracy. When the wave number lies in the pass bands, some traveling Bloch waves appear. To guarantee a well-posed PDE problem, one has to specify a physically-relevant radiation condition. How to extend the proposed method for this case is an interesting problem.

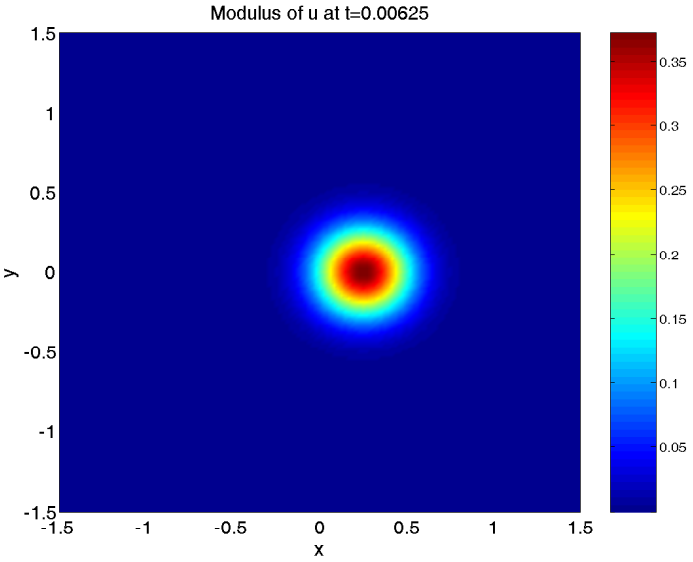

Fig. 15: $V_0 = 0$.

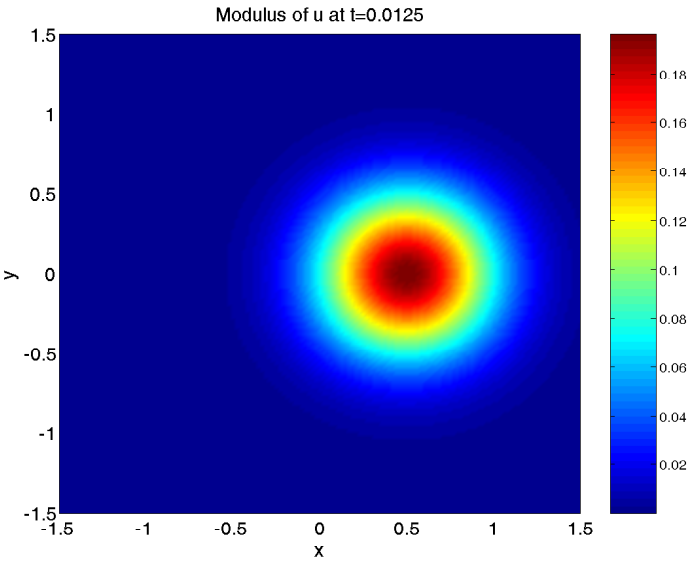

Fig. 16: $V_0 = 0$.

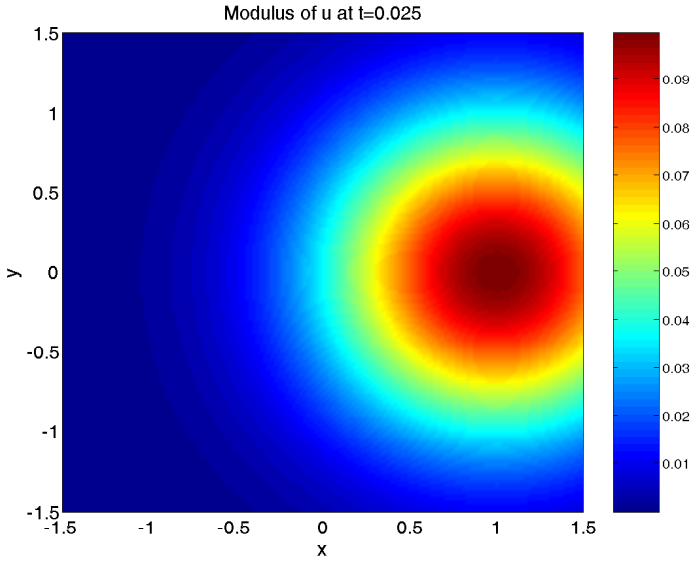

Fig. 17: $V_0 = 0$.

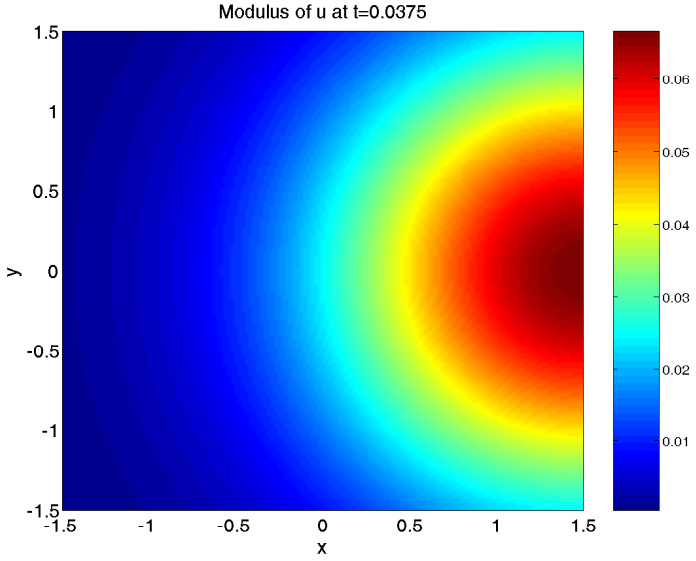

Fig. 18: $V_0 = 0$.

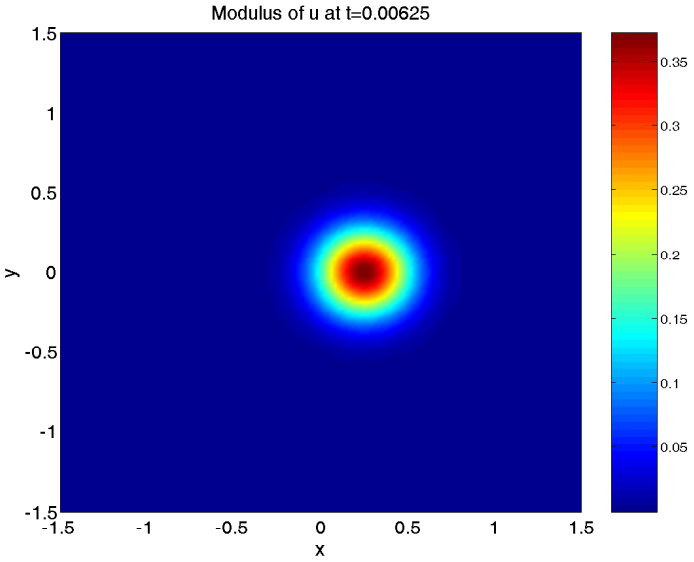

Fig. 19: $V_0 = 4000$.

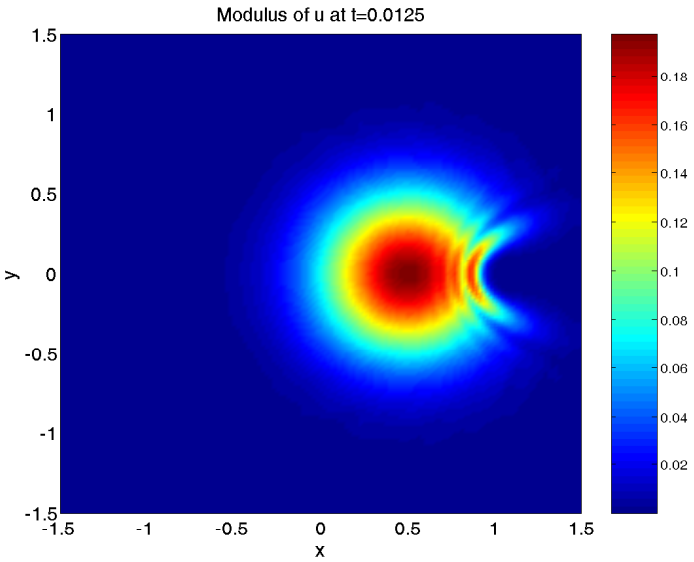

Fig. 20: $V_0 = 4000$.

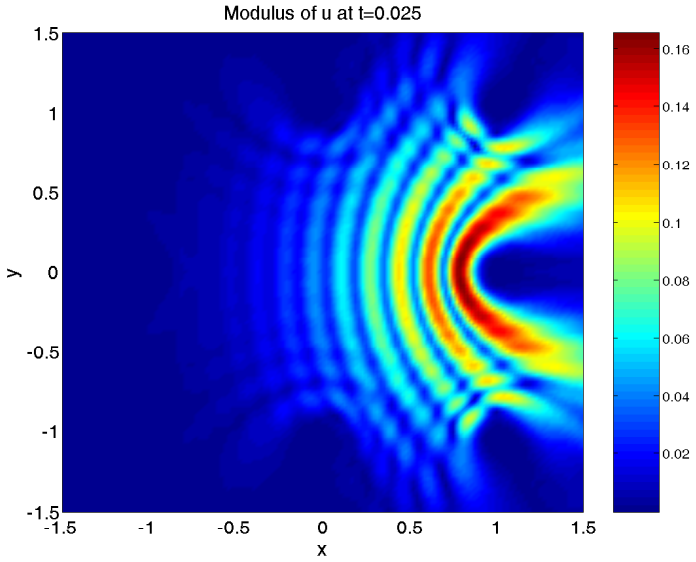

Fig. 21: $V_0 = 4000$.

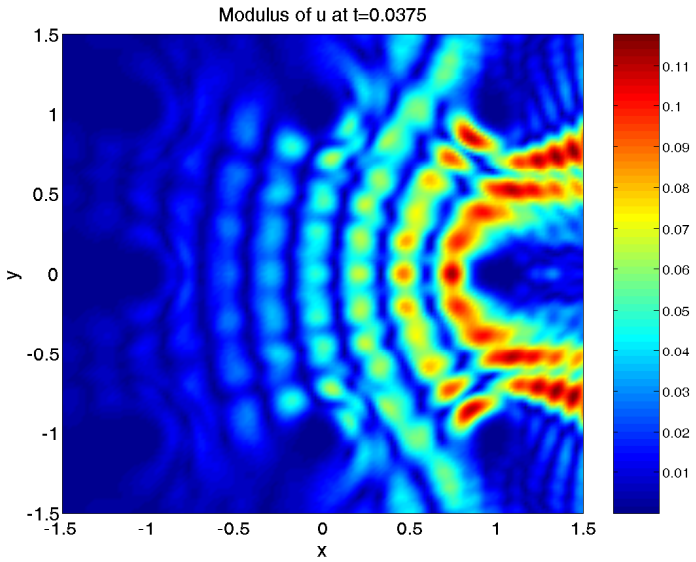

Fig. 22: $V_0 = 4000$.

Acknowledgments

The authors would like to thank Prof. Xavier Antoine for some stimulating discussions.

Appendix

Lemma A. The following Helmholtz equation is uniquely solvable for any $f_0, g_N \in (H^{1/2}(\Gamma_0))'$ and any $z \in \mathbb{Z}\backslash\{0\}$

$$\begin{aligned}
&-\Delta u(\mathbf{x}) + z n^2 u(\mathbf{x}) = 0,\ \mathbf{x} \in \Omega \equiv \cup_{i=0}^{N-1} C_i,\\
&\partial_y u(\mathbf{x}) = 0,\ \mathbf{x} \in \cup_{i=0}^{N-1} \Sigma_i^{\pm},\\
&-\partial_x u(\mathbf{x}) + \sqrt[+]{z}\, u(\mathbf{x}) = f_0,\ \mathbf{x} \in \Gamma_0,\\
&\partial_x u(\mathbf{x}) + \sqrt[+]{z}\, u(\mathbf{x}) = g_N,\ \mathbf{x} \in \Gamma_N,
\end{aligned}$$

where $n \in C^1(\cup_{i\in\mathbb{Z}} C_i)$, C_i and $\Sigma_i^{\pm}$ are defined as in Fig. 1.

Proof. The weak form of the above equation is:
Find $u \in H^1(\Omega)$, such that

$$a(u,v) = F(v),\ \forall v \in H^1(\Omega),$$

where

$$a(u,v) = (\nabla u, \nabla v) + z(n^2 u, v) + \sqrt[+]{z}(u,v)_{\Gamma_0} + \sqrt[+]{z}(u,v)_{\Gamma_N}$$

and

$$F(v) = < f_0, v >_{\Gamma_0} + < g_N, v >_{\Gamma_N},\ \forall v \in H^1(\Omega).$$

If $\mathrm{Im}\, z \neq 0$ or z is a positive real number, $a(\cdot,\cdot)$ is coercive in the space $H^1(\Omega)$. According to the Lax-Milgram theorem, the Helmholtz equation has a unique weak solution. If z is a negative real number, since the bilinear form $a(\cdot,\cdot)$ satisfies the Gårding inequality, the Fredholm alternative thus holds, which means we need only to prove the uniqueness. Take $f_0 = g_N = 0$ and $v = u$, and we get

$$(\nabla u, \nabla u) + z(n^2 u, u) + \sqrt[+]{z}(u,u)_{\Gamma_0} + \sqrt[+]{z}(u,u)_{\Gamma_N} = 0,$$

which implies $u = 0$ on $\Gamma_0 \cup \Gamma_N$. Since $f_0 = g_N = 0$ we also have $\partial_x u = 0$ on $\Gamma_0 \cup \Gamma_N$. Let us define

$$\tilde{u} = \begin{cases} u & , \mathbf{x} \in \Omega = \cup_{i=0}^{N-1} C_i, \\ 0 & , \mathbf{x} \in \cup_{i \notin [0,N-1]} C_i. \end{cases}$$

Then $\tilde{u} \in H^1_{loc}(\cup_{i\in\mathbb{Z}} C_i)$ satisfies the Helmholtz equation. According to the unique continuation principle (see page 64 in [26]), we have $\tilde{u} \equiv 0$, thus $u \equiv 0$. □

Lemma B. The operators $I - \mathcal{A}_m \mathcal{D}_n$ and $I - \mathcal{D}_n \mathcal{A}_m$ are invertible.

Proof. We only prove the invertibility of $I-\mathcal{A}_m\mathcal{D}_n$. It suffices to show that if $(I-\mathcal{A}_m\mathcal{D}_n)g=0$, i.e., $\mathcal{A}_m\mathcal{D}_ng=g$, then $g=0$. Let us denote by u_1 the solution of the Helmholtz equation on $\cup_{i=0}^{n-1}C_i$ with the boundary conditions

$$\mathcal{F}_{u_1}^x|_{\Gamma_0}=0, \qquad \mathcal{G}_{u_1}^x|_{\Gamma_n}=g.$$

In addition, we denote by u_2 the solution of the Helmholtz equation on $\cup_{i=n}^{n+m-1}C_i$ with the boundary conditions

$$\mathcal{F}_{u_2}^x|_{\Gamma_n}=\mathcal{D}_ng, \qquad \mathcal{G}_{u_2}^x|_{\Gamma_{m+n}}=0.$$

In terms of the definitions of $\mathcal{A}_i$ and $\mathcal{D}_i$ we have

$$\mathcal{F}_{u_1}^x|_{\Gamma_n}=\mathcal{D}_ng, \qquad \mathcal{G}_{u_2}^x|_{\Gamma_n}=\mathcal{A}_m\mathcal{D}_ng=g.$$

Thus then,

$$\mathcal{F}_{u_1}^x|_{\Gamma_n}=\mathcal{F}_{u_2}^x|_{\Gamma_n}, \qquad \mathcal{G}_{u_1}^x|_{\Gamma_n}=\mathcal{G}_{u_2}^x|_{\Gamma_n}.$$

This implies that if we define

$$u=\begin{cases} u_1 & , \mathbf{x}\in\cup_{i=0}^{n-1}C_i, \\ u_2 & , \mathbf{x}\in\cup_{i=n}^{n+m-1}C_i, \end{cases}$$

then u solves the Helmholtz equation on $\cup_{i=0}^{n+m-1}C_i$. Since

$$\mathcal{F}_u^x|_{\Gamma_0}=\mathcal{F}_{u_1}^x|_{\Gamma_0}=0, \qquad \mathcal{G}_u^x|_{\Gamma_{n+m}}=\mathcal{G}_{u_2}^x|_{\Gamma_{n+m}}=0,$$

according to Lemma A, we have $\tilde{u}\equiv 0$ and thus $g=0$. □

References

[1] T. Abboud, Electromagnetic waves in periodic media, in: R. Kleinman, T. Angell, D. Colton, F. Santosa and I. Stakgold (Eds.), Proceedings of the Second International Conference on Mathematical and Numerical Aspects of Wave Propagation, Newark, DE, 1993, SIAM, Philadelphia, 1993, pp. 1-9.

[2] B. Alpert, L. Greengard and T. Hagstrom, Nonreflecting boundary conditions for the time-dependent wave equation, J. Comput. Phys. 180 (2002), 270-296.

[3] X. Antoine, A. Arnold, C. Besse, M. Ehrhardt and A. Schädle, *A Review of Transparent and Artificial Boundary Conditions Techniques for Linear and Nonlinear Schrödinger Equations*, Commun. Comput. Phys. 4 (2008), 729-796.

[4] F. M. Arscott, Periodic differential equations, Pergamon Press, Oxford, 1964.

[5] M. Barth and O. Benson Manipulation of dielectric particles using photonic crystal cavities, Appl. Phys. Lett. 89 (2006), 253114.

[6] G. Bastard, Wave mechanics applied to semiconductor heterostructures, les éditions de physique, Les Ulis Cedex, France, 1988.

[7] P. Bienstman and R. Baets, Optical modelling of photonic crystals and VCSELs using eigenmode expansion and perfectly matched layers, Opt. Quant. Electron. (33) (2001), 327-341.

[8] M. Ehrhardt, Discrete Artificial Boundary Conditions, Dissertation, TU Berlin, 2001.
[9] M. Ehrhardt and C. Zheng, Exact artificial boundary conditions for problems with periodic structures, Preprint No. 27–2007 of the Institute for Mathematics, TU Berlin, July 2007, J. Comput. Phys., submitted.
[10] S. Fliss and P. Joly, *Exact boundary conditions for time-harmonic wave propagation in locally perturbed periodic media*, to appear: Appl. Numer. Math., 2008 (Special Issue of WONAPDE 2007: The Second Chilean Workshop on Numerical Analysis of Partial Differential Equations, Concepción, Chile, January 16-19, 2007).
[11] W. M. C. Foulkes, L. Mitas, R. J. Needs und G. Rajagopal, Quantum Monte Carlo simulations of solids, Rev. Mod. Phys. 73 (2001), 33-83.
[12] C. Fox, V. Oleinik and B. Pavlov, A Dirichlet-to-Neumann map approach to resonance gaps and bands of periodic networks, In: N. Chernov, Y. Karpeshina, I. W. Knowles, R. T. Lewis and R. Weikard (Eds.), Recent advances in differential equations and mathematical physics, volume 412 of Contemp. Math., pp. 151-169. Amer. Math. Soc., Providence, RI, 2006.
[13] H. Galicher, Transparent boundary condition for the one-dimensional Schrödinger equation with periodic potentials at infinity, Commun. Math. Sci., submitted.
[14] D. Givoli, Non-reflecting boundary conditions, J. Comput. Phys. 94 (1991), 1-29.
[15] D. J. Griffiths and C. A Steinke, Waves in locally periodic media, Am. J. Phys. 69 (2001), 137-154.
[16] H. Han, The artificial boundary method-numerical method of partial differential equations on unbounded domains, in Frontiers and Propests of Contemporary Applied Mathematics, edited by T. Li and P.Zheng, Higher Education Press, World Scientific, 2005, 33-58.
[17] T. Hagstrom, Radiation boundary conditions for the numerical simulation of waves, Acta Numerica 8 (1999), 47-106.
[18] Z. Han, E. Forsberg and S. He, Surface plasmon Bragg gratings formend in metal-insulator-metal waveguides, IEEE Photonics Techn. Lett. 19 (2007), 91-93.
[19] S. F. Helfert and R. Pregla, Efficient analysis of periodic structures, J. Lightwave Technology 16 (1998), 1694-1702.
[20] P. L. Ho and Y. Y. Lu, A bidirectional beam propagation method for periodic waveguides, IEEE Photonics Techn. Lett. 14 (2002), 325-327.
[21] J. Jacobsen, Analytical, numerical, and experimental investigation of guided waves on a periodically strip-loaded dielectric slab, IEEE Trans. Antennas and Propagation 18 (1970), 379-388.
[22] S.G. Johnson and J.D. Joannopoulos *Photonic crystals : the road from theory to practice* Kluwer Academic Publishers, 2002.
[23] P. Joly, J.-R. Li and S. Fliss, Exact Boundary Conditions for Periodic Waveguides Containing a Local Perturbation, Commun. Comput. Phys. 1 (2006), 945-973.
[24] P. Kuchment, Floquet theory for partial differential equations, volume 60 of Operator Theory: Advances and Applications, Birkhäuser Verlag, Basel, 1993.
[25] P. Kuchment, The mathematics of photonic crystals, Chapter 7 in: Mathematical modeling in optical science, volume 22 of Frontiers in applied mathematics, SIAM, Philadelphia, 2001.
[26] R. Leis, Initial boundary value problems in mathematical physics, Stuttgart: B.G. Teubner, Chichester, New York: Wiley, 1986.
[27] S. Li and Y.Y. Lu, Computing photonic crystal defect modes by Dirichlet-to-Neumann maps, Optics Express /15 (2007), 14454-14466.
[28] B. E. Little and H. A. Haus, A variational coupled-mode theory for periodic waveguides, IEEE J. Quantum Elect. 31 (1995), 2258-2264.

[29] K. Sakoda, Optical Properties of Photonic Crystals, Springer-Verlag, Berlin, 2001.
[30] I. A. Semenikhin, B. S. Pavlov and V. I. Ryzhii, Plasma waves in two-dimensional electron channels: propagation and trapped modes, Preprint No. NI07028-AGA of the Isaac Newton Institute for Mathematical Sciences, 2007.
[31] D. R. Smith, J. B. Pendry and M. C. K. Wiltshire, Metamaterials and Negative Refractive Index, Science 305 (2004), 788-792.
[32] T. Søndergard, S. I. Bozhevolnyi and A. Boltasseva, Theoretical analysis of ridge gratings for long–range surface plasmon polaritons, Phys. Rev. B 73 (2006), 045320.
[33] J. Tausch and J. Butler, Floquet Multipliers of Periodic Waveguides via Dirichlet-to-Neumann Maps, J. Comput. Phys. 159 (2000), 90-102.
[34] J. Tausch and J. Butler, Efficient Analysis of Periodic Dielectric Waveguides using Dirichlet-to-Neumann Maps, J. Opt. Soc. Amer. A 19 (2002), 1120-1128.
[35] S. V. Tsynkov, Numerical solution of problems on unbounded domains. A review., Appl. Numer. Math. 27 (1998), 465-532.
[36] A. Wacker, Semiconductor Superlattices: A model system for nonlinear transport, Phys. Rep., 357 (2002), 1-111.
[37] L. Yuan and Y. Y. Lu, An efficient bidirectional propagation method based on Dirichlet-to-Neumann maps, IEEE Photonics Techn. Lett. 18 (2006), 1967-1969.
[38] L. Yuan and Y. Y. Lu, Dirichlet-to-Neumann map method for second harmonic generation in piecewise uniform waveguides, J. Opt. Soc. of Am. B 24 (2007), 2287-2293.
[39] L. Yuan and Y. Y. Lu, A Recursive Doubling Dirichlet-to-Neumann Map Method for Periodic Waveguides, J. Lightwave Technology, 25 (2007), 3649–3656.
[40] J. Yuan, Y. Y. Lu and X. Antoine, Modeling photonic crystals by boundary integral equations and Dirichlet-to-Neumann maps, J. Comput. Phys. /227 (2008), 4617-3629.
[41] C. Zheng, Approximation, stability and fast evaluation of an exact artificial boundary condition for the one-dimensional heat equation, J. Comput. Math. 25 (2007), 730-745.
[42] C. Zheng, An exact boundary condition for the Schrödinger equation with sinusoidal potentials at infinity, Commun. Comput. Phys. 3 (2007), 641-658.